Anodic arc evaporation of nanocrystalline Mg films

O. FILIPOV, S. SCHIPPOREIT, V. BUCK*
University of Duisburg-Essen and CENIDE, Department of Physics, Thin Film Technology, Lotharstraße 1, Duisburg D-47057, Germany

This work aims at analysing the influence of bias voltage and hydrogen admixture on Mg grain size. The grain size was varied down to 18 nm. Also, using Monte Carlo simulations, it was shown that arc deposition is less aggressive against sensitive polymers than sputter deposition due to ion energies. The manipulation of magnesium grain size by variation of bias voltage and thus ion energies, and the influence of an admixture of hydrogen into the plasma was investigated using retarding field analysis and XRD. Possible applications for hydrogen storage are discussed.

(Received October 4, 2011; accepted April 11, 2012)

Keywords: Anodic arc, Arc evaporation, Ion energies, Mg, grain size, Hydrogen storage

1. Introduction

Hydrogen is an excellent, cheap and clean carrier for storage, conveyance and transformation of energy. The key problem is hydrogen storage. Metal hydrides are a challenging and safe alternative to storage in pressurised or liquid form [1,2]. Magnesium hydride MgH_2 combines a high hydrogen capacity of 7.6 wt % [3] (exceeds all known reversible metal hydrides) with the benefit of the low cost of the largely available magnesium. Many approaches were reported, mainly involving alloying magnesium with other elements, high energy or reactive ball milling of Mg, or surface modification of magnesium [2-5]. The influence of grain boundaries on hydrogen diffusion in Mg films has been investigated by [6,7]. They pointed out that nanocrystalline thin films have the advantage that on the one hand grain size is a crucial factor for hydrogen diffusion and on the other hand hydrogen loading and hydrogen kinetics are more efficient in thin films than in bulk Mg.

For large scale application Mg films should be deposited on polymer films and capped with e.g. a 20 nm Pd layer. To allow hydrogen loading from both sides, the hydrogen permeation through the polymer should not be reduced by the deposition process. Mg thin films can be obtained by many deposition methods. But a very economic way is to use high rate PVD (physical vapor deposition) technique. The commonly used method to produce films with high adhesion to survive hydrogen loading and unloading processes is sputtering. But vacuum arcs have orders of magnitude higher deposition rates. Both of these methods are well established in metallic thin film deposition field, but the deposition conditions like working gas pressure or particle energy are rather different. That determines their possibilities of application. The comparison in terms of impact of particle energy on polymer substrates for these two methods will be carried out below.

Thus in this work the influence of process parameters on the grain size of magnesium films deposited by anodic arc technique has been worked out.

2. Characterisation of the anodic arc

An industrial high vacuum chamber PLS Classic 500 (Pfeiffer Vacuum) equipped with an anodic vacuum arc source [8-10] was used for the experiments. The arc discharge can be operated in any vacuum condition since it is independent from operation gases, allowing to operate even in high vacuum.

A schematic diagram of the vacuum chamber and electrodes is shown in Fig. 1.

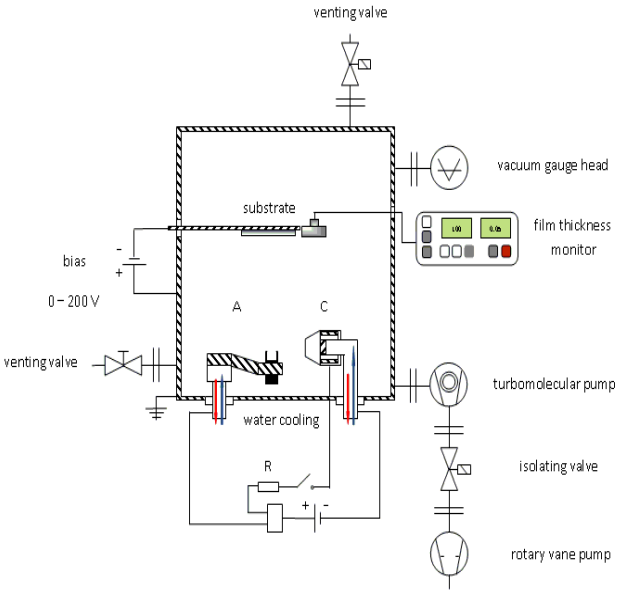

Fig. 1. Vacuum chamber, schematic diagram.

Cathode and anode are located in the vacuum chamber and connected to a water cooling system. The electrodes shown in Fig. 2 are insulated from the grounded chamber.

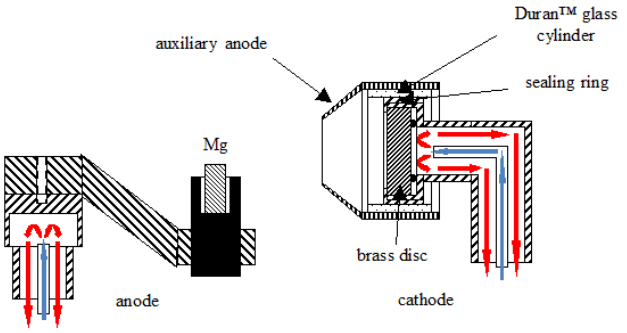

Fig.2. Schematic diagram of electrode construction.

The cathode consists of a water-cooled metallic disc, a sealing ring and a cone-shaped auxiliary anode, which is potentially separated from the cathode by a metal coated Duran™ glass (borosilicate glass with a low coefficient of thermal expansion) cylinder.

The anode consists of a crucible mounted on the water-cooled electrical feedthrough. In our experiments a graphite crucible was used. Anodic arc means that, in contrast to the common cathodic arc, anode material is deposited, while the cathode is used as an ionisation source solely. Cathode activity is also needed to transport the current from the cathode to the anodic plasma. In order to have a constant deposition rate from the anode it is necessary to keep a constant power flux to the anode. For this purpose one has to restrict the surface of the cathodic spot inside the central part of the cathode disc. This can be done in two ways: by using a sealing ring or by magnetic control of the cathodic spot [11,12]. The material of the sealing ring should have a much higher ignition voltage than the cathodic material. In our experiments, brass was used as cathode material because of low ignition current and effective cooling [12]. The restriction of the cathodic spot at the brass cathode is done with a molybdenum auxiliary anode which is potentially separated from the cathode by a Duran™ glass cylinder. Molybdenum was used because of its high melting point and because the burning voltage of the cathodic spot on it is much higher in comparison to the cathodic material. As was shown by [13], cathodic spot restriction is so effective that no magnetic control is necessary. In order to reduce erosion of cathodic material and to decrease the influence of the cathodic plasma onto the expanding anodic arc, the cone-shaped auxiliary anode orifice was made as small as possible [13]. During the plasma operation the temperature inside the auxiliary anode gets so high that backward evaporation of cathode material onto the cathode surface occurs, what leads to a reduction of cathode material erosion. The auxiliary anode also serves as a barrier against possible evaporation of cathode material.

The plasma is ignited with the help of the auxiliary anode. After applying current between the molybdenum auxiliary anode and the cathode, the thin metallic layer on the Duran™ glass cylinder evaporates due to ohmic heating [14] what ignites the auxiliary arc. After ignition, the electrons which leave the cathode are accelerated towards the anode by the potential difference between the electrodes. This results in rapid evaporation of the anode material and also its ionization. The anodic arc ignites when a critical evaporation rate is reached. Then the auxiliary arc electric circuit can be turned off [13].

During the deposition, the power input to the anode is concentrated on the molten material. Intense and bright colour of the evaporated metal in the plasma cloud around the anode prove strong activation (excitation and ionization) of the produced anodic arc plasma [14].

One big advantage of anodic and thermionic arcs compared to cathodic arcs is that there are no marcroparticles produced during the deposition due to the evaporation of the metal from the anodic crucible. Those marcroparticles are produced only at cathodic evaporation by moving cathodic spots.

Ion energies

Monte Carlo computer simulations have been performed in order to compare the impact of particle energies of the PVD methods sputtering and arc-deposition on sensitive substrate materials. These deposition methods are characterised by different kinds of plasmas. While sputter deposition is operated with an inert gas with kinetic ion energies around 1 keV, no working gas is needed for arc technology. Argon is the working gas which is used most often for sputtering. That is why argon was used for the calculations.

During sputtering, a certain number of argon ions are reflected at the target. Those of the reflected ions which capture an electron move towards the substrate, uninfluenced from the electric field, with virtually unchanged kinetic energies [15]. The results of the simulations show that the working gas in sputtering is aggressive against polymers.

For the calculations the program TRIM (Transport of Ions in Matter) was used. TRIM calculates the physical phenomena associated with the penetration of ions in matter [16]. Here, it is used to evaluate how ions which occur in sputter- and arc-deposition lose energy into a polymer. Detailed calculations were made with full damage cascades. For the evaluation, atom displacements and the electronic excitations of lattice atoms by collisions as well as the final ion distribution are considered. The polyimide Kapton™ was chosen, because its structure resembles the structures of polyimides which are used as hydrogen permeation membranes, and its atom stoichiometry is implemented in the program's compound dictionary. The number of ions was set to 100,000 for each simulation.

First, sputtering of $Pd_{77}Ag_{33}$ and of Mg by Ar ions was simulated. In average, 1.5 Mg atoms are sputtered by each Ar ion. After leaving the surface, the sputtered Mg atoms have a kinetic energy of 8 eV.

The second step is the coating of Mg (8 eV) on the polymer Kapton™. This simulation is valid for both, sputter and arc deposition methods, because the energies of Mg particles are in the same range. There are no atoms displaced in the polymer. Only ionisation takes place in the first nanometres. The collision events in Kapton™ caused by Mg are shown in Fig. 3.

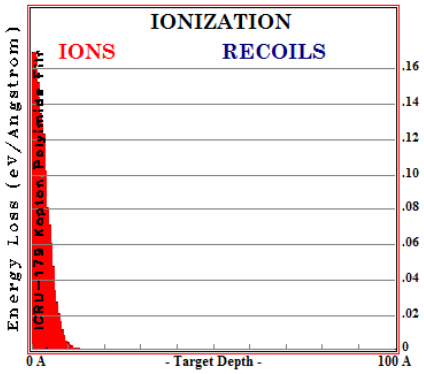

Fig 3. Collision events in Kapton™ caused by Mg particles.

In contrast to this, high-energy argon ions produce severe target damage up to a depth of 8 nm, as shown in Fig. 4. Most collisions produce vacancies, only a few atoms are replaced by argon.

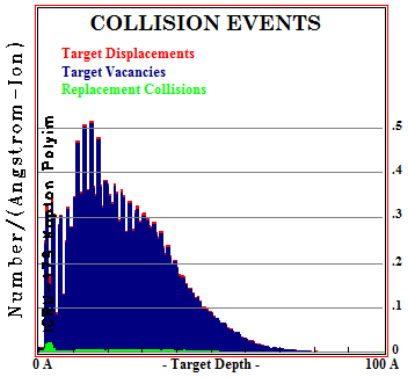

Fig 4. Collision events in Kapton™ caused by Ar ions.

One can conclude that the particles of the working gas in sputter deposition are aggressive against polymer films and damage is done in the bulk medium. If polymer films which allow hydrogen permeation, for example for loading or unloading Mg coated polymer films with hydrogen, arc technology should be preferred for coating.

3. Film deposition

The films were deposited onto 50x50 mm steel substrates. These substrates were pretreated in an ultrasonic bath with acetone to remove surface contaminations. Then the substrates were transferred into the vacuum chamber, which then was pumped down to a pressure of 10^{-7} mbar.

Variation of the process parameters substrate bias (from 0 V to 200 V) and hydrogen admixture (from 0 sccm to 1000 sccm) was used to influence the film properties. The bias voltage was changed in steps of 50 V. According to different hydrogen flow rates, different deposition pressures were obtained. This parameter is also very important for plasma chemistry, because it influences the particle energy, and in turn particle activity and film properties [17]. In Tab. 1 the corresponding deposition parameters are listed.

Tab. 1. Working pressure in dependence on hydrogen flow rate.

Hydrogen flow rate, (sccm)	0	220	700	1000
Working pressure, (mbar)	5×10^{-7}	1×10^{-4}	5×10^{-4}	1×10^{-3}

During the deposition, plasma parameters were monitored by a retarding field energy analyser and a mass-spectrometer.

4. Plasma analysis

Plasma composition

Before every deposition process and during the deposition, the gas composition was measured. The deposition process was monitored using QMS-200 Prisma by Balzers™. Fig. 5 shows a characteristic residual gas spectrum before deposition at a pressure of 1×10^{-7} mbar.

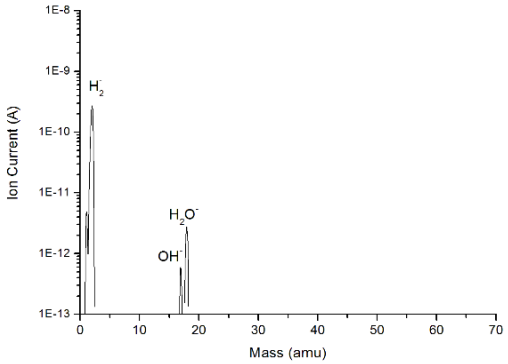

Fig. 5. Residual gas mass-spectrum.

Only hydrogen and water can be found in the mass-spectrum. This is a typical high vacuum residual gas spectrum. Fig. 6 shows the mass-spectrum during Mg deposition with 220 sccm hydrogen flow rate at 1×10^{-4} mbar working pressure.

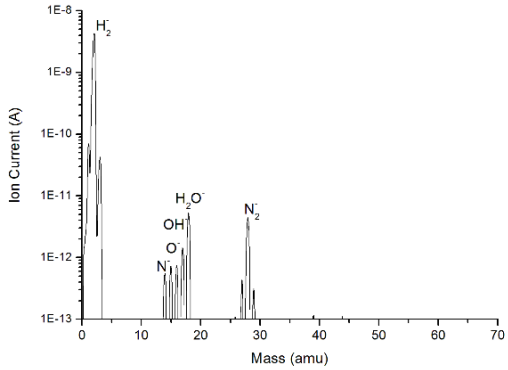

Fig. 6. Working atmosphere mass-spectrum.

The presence of the oxygen and nitrogen peaks can be ascribed to surface desorption of nitrogen during plasma operation because of high temperature of the graphite crucible. The absence of argon and oxygen peaks at 40 and 32 amu correspondingly implies that there is no leak or contamination coming from the gas transport system. Mg is not detected because it condenses at the wall and, thus, does not reach the spectrometer.

Ion energy

Energy resolved ion current measurements were performed with retarding field plasma analysis [18-22]. The energy analyser was mounted at the substrate position, which allows monitoring of deposition processes near the substrate. In [23] it was shown that the particle flux from the plasma to the analyser is identical to the particle flux to the grounded substrate during deposition. That is why ion energy measurements were done only without bias voltage. The results of the measurements are shown below in Fig.7 and Fig. 8.

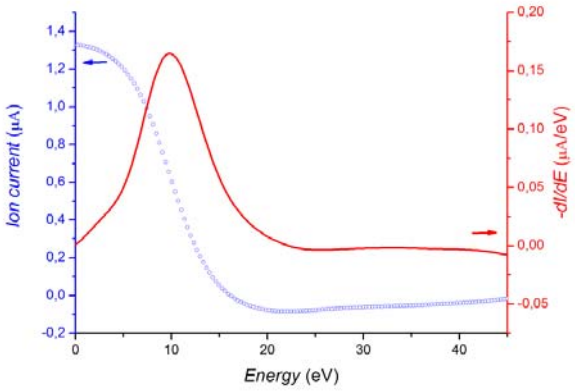

Fig. 7. Measured ion current and derived ion energy for magnesium coating (0 V bias, 0 sccm hydrogen flow rate).

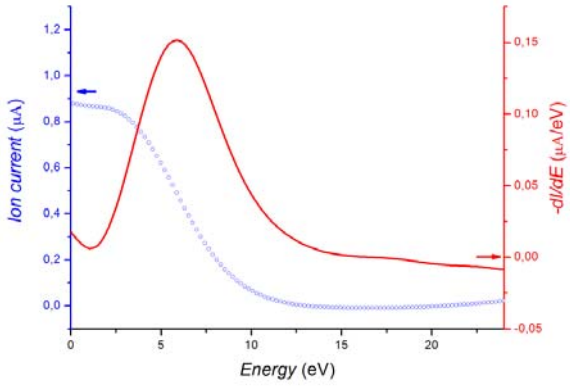

Fig. 8. Measured ion current and derived ion energy for magnesium coating (0 V bias, 1000 sccm hydrogen flow rate).

It was found that due to the introduction of hydrogen, the ion energy changes. Ions now experience more collisions on the way to the substrate (see Fig. 9).

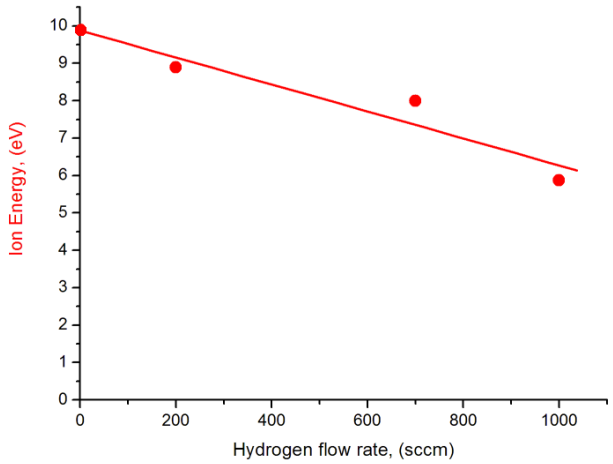

Fig. 9. Measured ion energy of deposited Mg ions as a function of hydrogen flow rate.

5. Film analysis

EDX

Energy dispersive X-ray (EDX) spectrum imaging has been performed on scanning electron microscope Quanta 400 FEG equipped with EDAX analyse system type "Genesis 4000" using an acceleration voltage of 15 kV. Magnesium coated steel substrates were analysed to characterise their elemental distribution.

Negligible amounts of impurities from the brass cathode (Cu and Zn) can be found in the Mg films. A comparison of an uncoated (Fig. 10) and a coated steel substrate (Fig. 11).

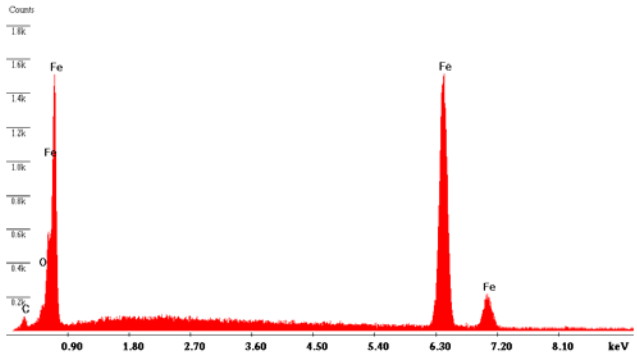

Fig. 10. EDX spectrum of an uncoated steel substrate.

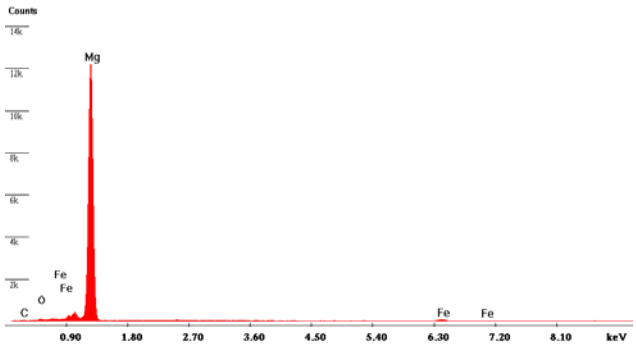

Fig. 11. EDX spectrum of a magnesium coated steel substrate.

Fig. 11 shows that a small peak appears around 1 keV. This peak can be attributed to Zn and Cu (or to Na impurities of the magnesium used for coating).

In Fig. 12 and Fig. 13 one can see the eroded surface of the cathodic disc (brass cylinder).

Fig. 12. Picture of the cathode disc.

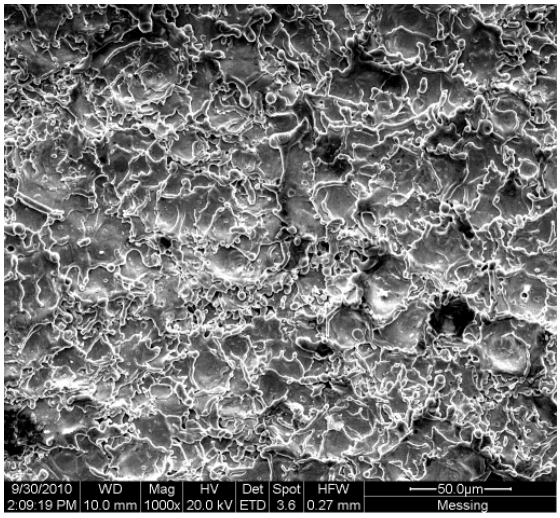

Fig. 13. SEM picture of the eroded cathode disc.

The presence of the Mg peak in Fig. 14 indicates that evaporated anodic material is also deposited onto the cathode surface, what decreases plasma and film contamination by the cathode material.

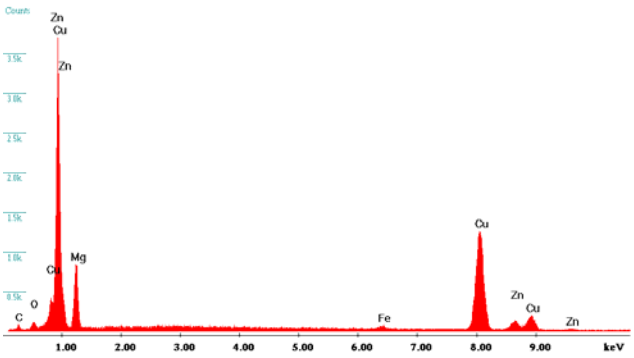

Fig. 14. EDX spectrum of the brass cathode.

SEM

To investigate surface morphology of the deposited films, the scanning electron microscope (SEM) ESEM Quanta 400 FEG by FEI Company was used. Using SEM pictures one can estimate the morphology and grain size of deposited magnesium crystallites.

The grain size of a specimen coated at a working pressure of 1×10^{-4} mbar is around 50 nm (see Fig. 15), what is in a good agreement with the evaluation from the XRD patterns.

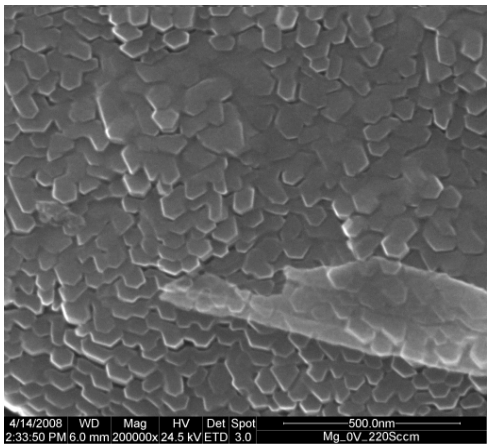

Fig. 15. SEM picture of the coated specimen. Bias 0 V, working pressure: 1×10^{-4} mbar.

XRD

XRD was used to determine the grain size of the coatings. The X-ray diffraction profiles were recorded with a Bruker AXS D8 diffractometer using CuK_{α} radiation. Small crystallite size and crystal imperfection or defects (vacancies, dislocations, grain boundaries and voids) are commonly considered to be a reason for broadening of diffraction peaks.

Broadening of diffraction peaks arises mainly due to two factors: small crystallite size and lattice strain. These factors transform a perfect peak (peak without width) into an observed broadened peak (see Fig. 16).

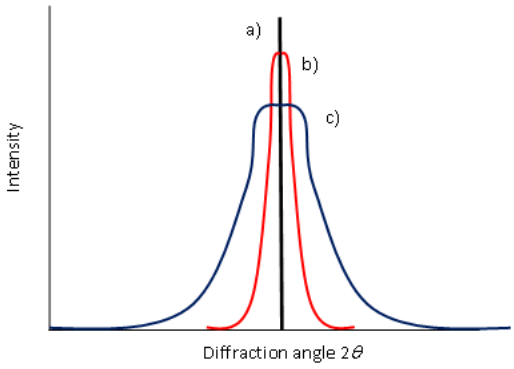

Fig. 16. Broadening of X-ray diffraction peaks: a) perfect peak, b) peak broadening due to small crystallite size, c) peak broadening caused by lattice strain effects [24].

However, there is a method to separate these factors. Scherrer [25] has derived an equation for broadening of X-ray diffraction peaks due to small crystallite size:

$$B_{crystallite} = \frac{k\lambda}{G \cdot \cos\theta}, \quad (1)$$

where λ is the wavelength of X-rays used (λ = 0,15406 nm), θ is the Bragg angle, G is the "average" crystallite size, k is a constant (in our case k = 0,94).

The lattice strain ε in the deposited films also causes broadening of the diffraction peaks, which can be described by [26]:

$$B_{strain} = \varepsilon \cdot \tan\theta, \quad (2)$$

where $\varepsilon = \Delta d/d$ is the strain in the material. Using equations (1) and (2), one can see that peak broadening increases rapidly with increasing θ, and that separation between these two factors is clearer at smaller θ values (see Fig. 17). The width B_I, the full width at half maximum (FWHM) of the diffraction peak, can be considered as the sum of widths due to small crystallite sizes and lattice strains:

$$B_I = B_{crystallite} + B_{strain}. \quad (3)$$

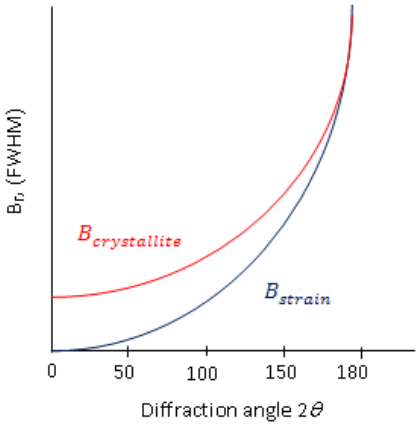

Fig. 17. Dependence of FWHM caused by small crystallite size and lattice strain on the diffraction angle [24].

From equations (1), (2) and (3) we get:

$$B_I = \frac{k\lambda}{G \cdot \cos\theta} + \varepsilon \cdot \tan\theta. \quad (4)$$

Equation (4) multiplied by $\cos\theta$ is:

$$B_I \cos\theta = \frac{k\lambda}{G} + \varepsilon \cdot \sin\theta. \quad (5)$$

If we now plot $B_I \cdot \cos\theta$ against $\sin\theta$ we obtain a straight line with slope ε and intercept $k \cdot \lambda / G$. This method is called Williamson-Hall plot [27]. The smaller the value of ε, the flatter the straight line, the smaller is the strain in the sample. Then the crystallite size G can be calculated from the intercept by using values of k and λ mentioned above.

Fig. 18 shows the XRD spectrum for a magnesium coating and Fig. 19 shows the evaluation of XRD profiles using a Williamson-Hall plot. From that one can deduce the grain size.

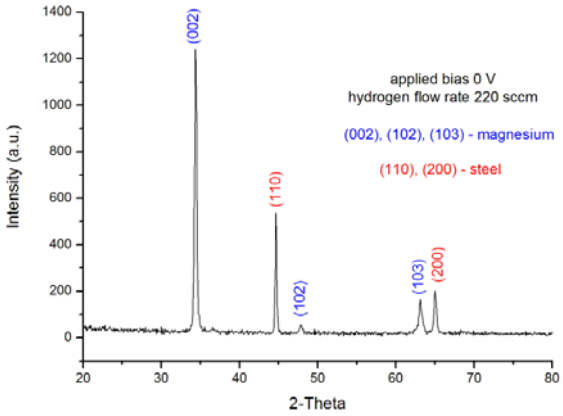

Fig. 18. XRD pattern of Magnesium coated steel specimen, with peaks evaluation.

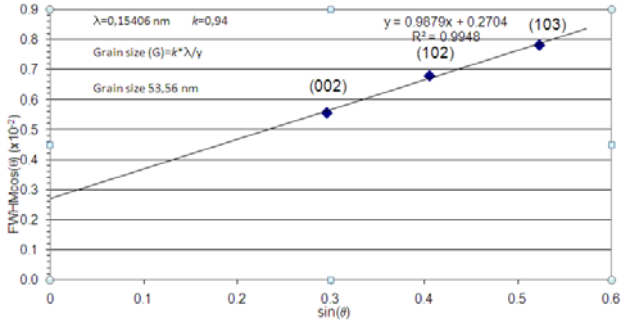

Fig. 19. Williamson-Hall plot.

In [28] deposition of Mg films by sputtering in hydrogen containing argon atmosphere has been carried out. Because the anodic arc can be operated in hydrogen atmosphere, too, the influence of hydrogen pressure during deposition has been analysed additionally.

Fig. 20 shows a summarised 3D-diagram of Mg grain size as a function of applied bias voltage and actual hydrogen flow rate.

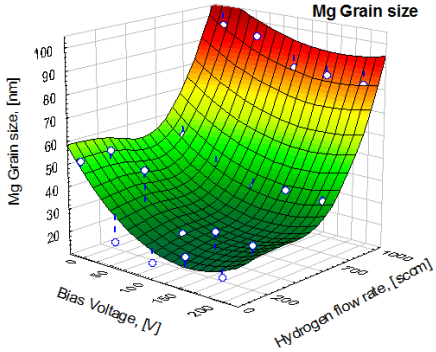

Fig. 20. Magnesium grain size as a function of deposition parameters.

As one can see in Fig. 20, the applied bias voltage leads to a reduction of the crystallite size due to ion peening. On the other hand, increasing hydrogen pressure leads to increased Mg grain size which can be due to thermalisation.

Obviously H is incorporated (determined) by SIMS, but increasing grain size reduces the scope of hydrogen kinetics.

6. Summary

Bias voltage was varied in order to vary Mg grain size during anodic arc deposition.

It was shown that the grain size in the deposited films can be varied down to 18 nanometres by variation of deposition parameters. For application as storage material no hydrogen should be added to get minimal grain size.

References

[1] A. Zaluska, L. Zaluski, J. O. Strom-Olsen, Appl. Phys. A: Mater. Sci. Process., **72**(2), 157 (2001).
[2] J. Huot, G. Liang, R. Schulz, Appl. Phys. A: Mater. Sci. Process. **72**(2), 187 (2001).
[3] Rudy W. P. Wagemans, Joop H. van Lenthe, Petra E. de Jongh, A. Jos van Dillen, and Krijn P. de Jong, J. Am. Chem. Soc. **127**, 16675 (2005).
[4] H. Imamura, S. Nakatomi, K. Tanaka, Y. Hashimoto, Y. Sakata, Proceedings WHEC 2010, 319 (2010).
[5] Y. Q. Hu, H. F. Zhang, C. Yan, L. Ye, B. Z. Ding, Z. Q. Hu, J. Mater. Sci. **39**(4), 1455 (2004).
[6] A. Pundt and R. Kircheim, Annu. Rev. Mater. Res., **36**, 555 (2007).
[7] H. T. Uchida, R. Kirchheim, A. Pundt, Scr. Mater. **64**, 935 (2011).
[8] H. Ehrich, B. Hasse, M. Mausbach, K. G. Müller, IEEE Trans. Plas. Sci. **18**(6), 895 (1990).
[9] H.M. Katsch, M. Mausbach, K.G. Müller, J. Appl. Phys. **67**(8), 1 (1990).
[10] H. Ehrich, B. Hasse, K. G. Müller, Mater.
[11] H. Ehrich, B. Hasse, M. Mausbach, K. G. Müller, R. Schmidt, J. Vac. Sci. Technol. A **6**(4), 2499 (1988).
[12] H. Ehrich, J. Vac. Sci. Technol. A **6**(1), 134 (1988).
[13] B. Hasse, Dissertation, Dordrecht (1992).
[14] H. Ehrich, B. Hasse, M. Mausbach, K. G. Müller, Sci. Technol. A **8**(3), 2160 (1990).
[15] H. Matsui, H. Toyoda, H. Sugai, J. Vac. Sci. Technol. A **23**(4) (2005).
[16] J. F. Ziegler, Nucl. Instr. Meth. Phys. Res. B **219-220**, 1027 (2004).
[17] Y. P. Raiser: Gas discharge Physics, Springler-Verlag, Berlin/New York (2001).
[18] J. D. Stephanakis, W. H. Bennet, Rev. Sci. Instrum. **39**, 1714 (1968).
[19] G. S. Musa, H. Ehrich, M. Mausbach, J. Vac. Sci. Technol. A **12**, 2887 (1994).
[20] J. Schuhmann, Metallisierung von Polymeren, Shaker Verlag, Aachen (2000).
[21] G. S. Musa, H. Ehrich, J. Schuhmann, IEEE Transactions on Plasma science **23**(2), 386 (1997).
[22] C. Surdu-Bob, G. S. Musa, V. Buck, I. Mustata, O. Filipov, A. Poukhovoi, J. Optoelectron. Adv. Mater. **9**, 2657 (2007).
[23] S. Jäger, B. Szyszka, J. Szczyrbowski, G. Bräuer, Surface and Coatings Technology **98**, 1304 (1998).
[24] C. Suryanarayana, M. Grant Norton, X-ray diffraction - a practical approach, Plenum Press, New York (1998).
[25] P. Scherrer, Goettinger Nachrichten Gesell., **2**, 98 (1918).
[26] J. M. Cowley, Diffraction physics, North-Holland, Amsterdam (1975).
[27] G. K. Williamson, W. H. Hall, Acta Metall. **1**, 22 (1953).
[28] D. Milčius, L. Pranevičius, G. Thomas, M. Lelis, Mat. Sci. **10**(3), 217 (2004).

*Corresponding author: volker.buck@uni-due.de